Electronic Coupling in InP Nanoparticle Arrays

Matthew C. Beard,[†,||] Gordon M. Turner,[†] James E. Murphy,[‡,§] Olga I. Micic,[§] Mark C. Hanna,[§] Arthur J. Nozik,*[,‡,§] and Charles A. Schmuttenmaer*[,†]

Department of Chemistry, Yale University, 225 Prospect St., P.O. Box 208107, New Haven, Connecticut 06520-8107, Department of Chemistry and Biochemistry, University of Colorado, Campus Box 215, Boulder, Colorado 80309-0215, and Center for Basic Sciences, National Renewable Energy Laboratory, 1617 Cole Blvd., Golden, Colorado 80401-3393

ABSTRACT

Arrays and lattices formed from nanoparticles (NPs) present unique opportunities for new optoelectronic materials whose properties can be tuned by controlling the size of the individual NPs and their interparticle separation to effect strong inter-NP electronic coupling. Characterization of the interdot coupling as a function of interdot distance is essential. Using time-resolved THz spectroscopy, we report a six-fold increase in the transient photoconductivity in disordered arrays of 3.2 nm diameter InP NPs separated by 0.9 nm compared to arrays with 1.8 nm separation. Photoconductivity in the arrays is compared to that of isolated NPs and InP epilayers. The epilayer samples exhibit bulk transport behavior while the NP samples do not.

There has been an increasing amount of effort in the nanoscience community to design, construct, and characterize "artificial" solids formed from nanoparticles (NPs). Arrays and lattices formed from NPs exhibit properties that depend not only on the size of the individual NPs but also on the interaction between NPs as their separation distance is varied. The nature of charge transport in semiconductor nanoparticle arrays is of particular fundamental importance to the advancement of various NP technologies.

Semiconductor NPs, also called quantum dots, have received considerable attention due to their size-dependent properties; a well-known example is that the band gap increases as the radius of the NP decreases, blue-shifting the absorption and luminescence spectra.[1−3] NP sizes smaller than the Bohr radius (a_B) of bulk excitons strongly confine the carriers and lead to the formation of discrete energy levels in the NPs. Two and three-dimensional NP arrays can exhibit collective behavior if individual NPs couple to one another, and these so-called "artificial solids" are the basis for many proposed optoelectronic devices−for which the ultimate goal is to produce materials that retain the tunable size-dependent properties of individual NPs while exhibiting some degree of collective behavior, such as long-range high-mobility charge transport.

One of the fundamental parameters that governs long-range charge transport in NP arrays is the electronic coupling between the NPs. This interdot coupling is affected by the surface of the NP, the interdot potential barrier height, the distance between the NPs, and their size.[4] The coupling increases as the NP size and interparticle distance decrease. The surface quality and distance between the NPs are determined primarily by the surface-capping material, which can be an insulating organic ligand such as trioctlyphosphine oxide (TOPO) and/or a capping shell of a second semiconductor (core−shell quantum dots). The organic ligand and/or the semiconductor shell protects the NPs from agglomeration and chemical attack. It also passivates surface states by reducing surface defects and provides a method for tuning the interdot coupling by varying its length or chemical nature.

In this work, we investigate the interdot coupling by measuring the photoconductivity in disordered arrays of 3.2 nm diameter InP NPs as a function of separation distance using time-resolved THz spectroscopy. Two different organic capping groups are used: hexylamine, which leads to an average interdot distance of ∼0.9 nm, and oleylamine, which leads to an average interdot distance of ∼1.8 nm. Isolated 3.2 nm diameter NPs capped with TOPO and dispersed into toluene were also studied. We find that the photoconductivity

* Corresponding authors. E-mail: anozik@nrel.nrel.gov; charles.schmuttenmaer@yale.edu
† Yale University.
‡ University of Colorado.
§ National Renewable Energy Laboratory.
|| Present address: NIST, Optical Technology Division, Mail stop 8443, Gaithersburg, MD 20899.

increases dramatically in the sample with a 0.9 nm separation compared to the sample with an 1.8 nm separation. In addition, transient photoconductivity in epilayers of InP with 8 and 18 nm thickness was measured. These samples exhibit Drude-like conductivity indicative of bulk behavior, while the NP arrays do not.

Studies of metallic NP arrays have shown that the coupling increases as the separation between the NPs is decreased. Collier et al. observed a reversible insulator-to-metal transition as the separation of Ag NPs was decreased by compression in a Langmuir trough.[5,6] Terrill and co-workers found that the tunneling probability in Au NP arrays separated by organic ligands increases exponentially with decreasing interdot distance.[7] Similar studies in semiconductor NP arrays find that the photoconductivity is dominated by a tunneling mechanism whereby the photocreated exciton is ionized and the electron tunnels to an adjacent NP. The energy required to ionize the exciton decreases with increasing NP size and decreasing interdot distance.[8] Previous studies of disordered InP NP arrays find that the peak in the excitonic absorption spectrum red-shifts and broadens relative to that of the isolated dots. The redshift increases for decreasing interparticle spacing, indicative of delocalization of the excitonic wave function and the formation of extended states.[4,9]

Time-resolved THz spectroscopy (TRTS) is a powerful and relatively new method for measuring the transient photoconductivity in semiconducting nanomaterials because it provides a noncontact electrical probe with subpicosecond temporal resolution.[10−13] Charge carriers are created in the NPs by absorption of above-band gap photons, and these newly created carriers are subsequently probed with a THz pulse. The pump−probe delay time is varied to map out the time-dependent far-IR (THz) response. The probe THz pulses have bandwidth extending from 5 to 100 cm^{-1} (0.15−3 THz). The full complex-valued generalized permittivity, $\tilde{\epsilon}$, of the material under investigation is recovered and is related to the complex conductivity $\tilde{\sigma}$ by $\tilde{\epsilon} = \epsilon_s + i\tilde{\sigma}/\epsilon_0\omega$, where ϵ_s is the static dielectric constant, ϵ_0 is the permittivity of free space, and ω is the radial frequency. Carrier scattering times in semiconductors are typically on the order of 10 fs to 1 ps, causing large variations in $\tilde{\sigma}(\omega)$ at THz frequencies.[10−13]

The experimental apparatus has been described in detail elsewhere and will not be repeated here.[10] In summary, the visible pump (400 nm) and THz probe pulses originate from an amplified Ti:sapphire source producing 100 fs pulses with 800 μJ/pulse at 800 nm. About 50 μJ/pulse of 400 nm light (doubled fundamental) is lightly focused onto the sample with a spot size of about 6 mm diameter; all of the visible photons are absorbed by the sample. The spot size of the pump pulse is larger than that of the THz probe spot size (3−4 mm). The THz probe pulses are generated via optical rectification in a 1-mm ZnTe crystal and are detected via free space electrooptic sampling in another 1-mm ZnTe crystal. A lock-in amplifier is employed with an optical chopper that modulates the visible pump pulse; transient signals on the order of 1 part in 10^5 can be measured with S/N ratios on the order of 1 to 3 (in a single scan with a 10 ms time constant) with this technique.
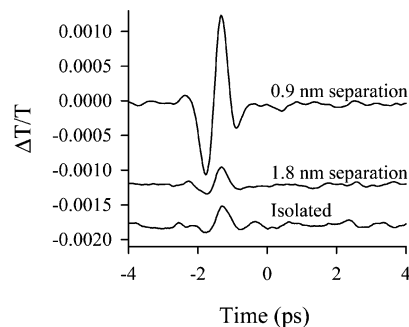
Figure 1. Difference plots of THz amplitude (pump on−pump off) at 1 ps pump−probe delay time. The traces have been vertically offset for clarity.

InP nanocrystals were synthesized by reacting $InCl_3$ with $P[Si(CH_3)_3]_3$ in a solution of trioctylphosphine oxide (TOPO) and trioctylphosphine(TOP) in a rigorously air-free and water-free environment. Size selective precipitation was used to narrow the size distribution of the NP colloid preparation to less than 10%. The TOPO cap was exchanged for the alkylamines by a simple ligand exchange procedure. Solid films of arrays of NPs were formed by carefully and slowly evaporating the colloidal dispersion in an octane−hexane solution onto a quartz substrate. The NP film thicknesses were measured with a profilimeter to be on average 6 μm and 15 μm for the 0.9 nm separation and 1.8 nm separation, respectively, and were highly nonuniform. The interdot distance in arrays of NPs with different organic capping groups was estimated from previously published data for close-packed NP arrays capped with organic ligands.[14,15] However, since hexylamine is a weak stabilizer with a relatively low boiling point, the NPs may partially lose their organic ligands so that the interdot distance may be slightly shorter than that estimated from the ligand length. A loss of ligand upon evaporation was recently reported for a close-packed film of 2.1-nm CdSe NPs, and it was found that this facilitated interdot electronic coupling.[16] The isolated samples were dispersed in toluene and measured in a 1 mm thick cuvette. Details of the NP colloid and array preparations are presented in refs 4 and 17.

The InP films of 8 and 18 nm thickness were prepared by chemical etching of epitaxial multilayer samples grown by metal organic chemical vapor deposition. The multilayer structures consisted of the thin InP film grown on a 0.3 μm thick InGaAs etch-stop layer that was lattice-matched to a (100) InP substrate. The sample was mounted with clear wax to a thin glass slide with the InP substrate exposed. Selective etchants were used to remove the InP substrate and the InGaAs layer, (HCl for InP, 2:1:10 $NH_4OH/H_2O_2/H_2O$ for InGaAs), leaving the thin InP epilayer supported by the glass slide.

Transient THz difference scans (pump-on minus pump-off) at a 1 ps pump−probe delay time for the three NP samples are displayed in Figure 1. The response of the sample with 0.9 nm separation is six times greater than that of the sample with 1.8 nm separation (which is essentially identical to the response of the isolated NP sample). This indicates an enhancement in the photoconductivity, with a

concomitant increase in THz absorption, when the interparticle distance is small enough to allow coupling.

Figures 2a and 2b display the frequency-dependent change in optical density (ΔOD) and change in phase ($\Delta\phi$), respectively, of the THz probe pulse 1 ps after photoexcitation of the sample. The frequency dependence provides detailed information about the conduction mechanism. We model only the 0.9 nm sample, treating it as a dielectric stack composed of air/photoexcited NPs/nonphotoexcited NPs/quartz, with a complex-valued transmission coefficient that depends on the properties and thickness of each layer.[11,12] The far-IR parameters of quartz have been measured in a separate experiment, and the nonphotoexcited NPs have a refractive index of 3.08[18] and negligible absorption and dispersion. If we assume that all the incoming pump photons create electron–hole (e–h) pairs and that only one e–h per NP is created, then there are the equivalent of ~60 NP layers excited. Thus, the thickness of the photoexcited layer is ~250 nm (60 × 4.1 nm). This is a reasonable assumption since the absorption cross section for InP NPs is 34.6 Å^2.[19] Contributions from multiply excited NPs are negligible. Incorporating an exponential decaying distribution of excited NPs would give a negligible correction to the calculation,[10,14] and for simplicity we treat this as equivalent to a slab of photoexcited NPs.

The Drude–Smith model of photoconductivity is used to describe the photoexcited NPs:[20]

$$\sigma(\omega) = \frac{\epsilon_0\,\omega_p^2\tau}{(1 - i\omega\tau)}\left[1 + \frac{c}{1 - i\omega\tau}\right] \qquad (1)$$

where τ is the carrier scattering time, ω is the radial frequency, c is the persistence of velocity parameter, and $\omega_p^2 = Ne^2/(\epsilon_0 m^*)$ is the plasma frequency, where N is the carrier density, e is the charge of an electron, and m^* is the effective mass of the carrier. The carrier density is assumed to be $1/V$ where V is the volume of the NPs. The term outside the brackets in eq 1 is the standard Drude conductivity, and the second term within the brackets allows for deviations from Drude-like behavior. The Drude model alone can *not* reproduce the measured data in either of the NP arrayed samples, even when a distribution of scattering times is incorporated. The value of c ($-1 < c < 0$) can be associated with the degree of backscattering that a carrier suffers after a collision. When $c = 0$ we recover the Drude model, and when $c = -1$ carriers undergo complete backscattering, which also corresponds to Anderson localization.[20,21] During the fit, we vary the scattering time, τ, the persistence of velocity parameter, c, and the thickness of the nonphotoexcited layer, d_{np}, whereas the thickness of the photoexcited layer is fixed at 250 nm. The smooth solid line through the 0.9 nm separation data in Figure 2 displays the best fit results.

Figure 3a displays the calculated photoconductivity based on the fit for the closely spaced array shown in Figure 2. For the arrays, the conductivity cannot be extracted because a numerical inversion of the corresponding relationship with ΔOD and $\Delta\phi$ is not stable. Therefore, we fit the above model to ΔOD and $\Delta\phi$ to extract the photoconductivity. In contrast,
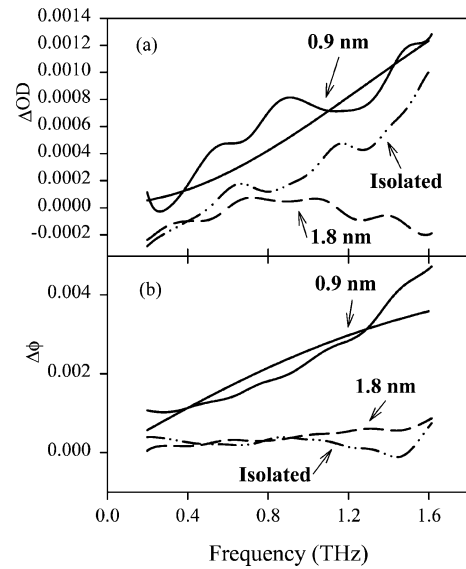

Figure 2. The change in OD (ΔOD), panel a, and change in phase ($\Delta\phi$), panel b, 1 ps after photoexcitation for the three NP samples. Solid line is for 0.9 nm separation, dashed line is for the 1.8 nm separation, and the dot–dot–dashed line is for the isolated NPs. The smooth solid lines are the calculated ΔOD and $\Delta\phi$ from the best fit of the Drude–Smith model to the 0.9 nm separation data.
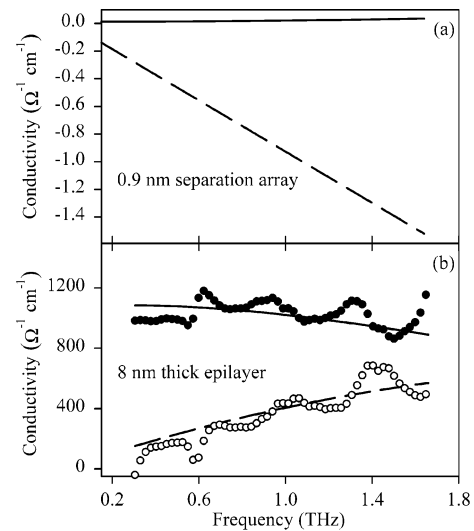
Figure 3. Panel (a) displays the real (solid line) and imaginary (dashed line) conductivity for the 0.9 nm separation NP array based on the parameters from the best fit of the Drude–Smith model to the data shown in Figure 2. Panel (b) displays the experimentally determined photoconductivity (Re[$\tilde{\sigma}$] − ●, Im[$\tilde{\sigma}$] − ○) for the 8 nm thick epilayer sample. The solid and dashed lines are real and imaginary conductivity, respectively, from the best fit of the Drude model.

the relationship between the conductivity and ΔOD and $\Delta\phi$ for the epilayers is less complicated, and we therefore first extract the conductivity and then fit the Drude model to the extracted values. The real conductivity of the arrays increases from 0.013 to 0.034 Ω^{-1}cm^{-1}, but this variation is too small to be seen on the scale of the plot in Figure 3a. The values of the best fit parameters are $d_{np} = 4.3\,(0.1)\,\mu$m, $c = -0.99994\,(0.00001)$, and $\mu = 17.258\,(0.082)$ cm^2 V^{-1} s^{-1}, where the mobility is related to the scattering time by $\mu = e\tau/m^*$, and $m^* = 0.07\,m_e$ for InP, with a corresponding
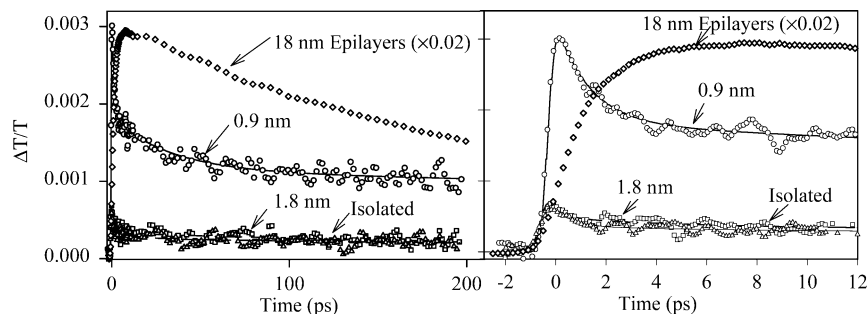
Figure 4. Pump dynamics of the three samples along with least-squares fitting results of a triexponential decay $y = [a_1 \exp(-t/\tau_1) + a_2 \exp(-t/\tau_2) + a_3 \exp(-t/\tau_3)] \otimes G$, where $\otimes G$ represents convolution with a Gaussian. Symbols are $\bigcirc$ − 0.9 nm separation, $\square$ − 1.8 nm separation, $\triangle$ − isolated samples, and $\diamond$ − 18 nm epilayers (scaled by 0.02). Solid lines represent the triexponential fits. Panel (a) displays the transients out to longer pump-delay times while panel (b) displays the short time transients.

scattering time of 0.69 fs. A value of c that is nearly -1 suggests that the long-range transport is severely restricted. This model cannot be adequately fit to the isolated NPs and 1.8 nm separation samples due to their extremely low absorption.

A typical dc-measurement of the conductivity, such as a four-point probe or time-of-flight measurement, assumes that $\sigma(\omega = 0) = \epsilon_0 \omega_p^2 \tau = eN\mu$, whereas the Drude−Smith model predicts a dc conductivity of $\sigma(\omega = 0) = eN\mu(1 + c)$. Therefore, a dc measurement of photoconductivity in the InP arrays would yield a mobility of 1.0×10^{-3} cm^2 V^{-1} s^{-1}: the fitted value of μ reduced by a factor of $(1 + c)$. Thus, the "dc" mobility in the arrays is reduced by a factor of 6.3×10^5 compared to that in the epilayer sample. A dc probe is sensitive to long-range mobility, whereas the THz probe reveals both long-range and local mobility. While the long-range transport is limited by inter-NP transport and hopping or tunneling of the carriers over large molecular distances, our measurements suggest that carriers remain locally conductive at high frequencies within one NP, or among several when they are electronically coupled.

In contrast to the NP arrays, photoconductivity in the InP epilayers does conform to the Drude model. Figure 3b displays the extracted photoconductivity and a fit of the Drude model to the conductivity for the 8 nm thick sample. A mobility of 650 cm^2 V^{-1} s^{-1} with a carrier density of 1.02×10^{19} cm^{-3} is obtained, which is consistent with literature values.[22] The conductivity is extracted from the measured ΔOD and $\Delta\phi$ as described in refs 10 and 11. The 8 and 18 nm epilayer samples show no substantial differences in their photoconductive responses. The carriers behave bulk-like, even when confined to less than the Bohr radius ($a_B = 10.8$ nm) in one dimension.

Figure 4 displays the time-dependence of the average THz response following photoexcitation of the NP samples and the 18 nm thick epilayer, normalized to a reference THz pulse. The data are collected by monitoring the peak of the THz pulse as a function of pump−probe delay.[10] The response of the 18 nm epilayer is 500 times greater than that of the NPs and has been scaled appropriately. The reduction in the photoconductivity of the NP array is due to confinement of the carriers in three dimensions. Each data set was fit to a triexponential decay function convoluted with

Table 1. Extracted Parameters from Nonlinear Least Squares Fit to Data Shown in Figure 4 (numbers in parentheses are 1 σ uncertainties)

	0.9 nm	1.8 nm	isolated
τ_1	1.33 (0.04)	0.42 (0.11)	0.715 (0.12)
τ_2	33. (1.)	6.3 (1.0)	13.7 (3.8)
τ_3	2035(10)	465(35)	880 (180)
a_1	0.49 (0.01)	0.53 (0.04)	0.60 (0.02)
a_2	0.19 (0.01)	0.16 (0.02)	0.11 (0.01)
$(a_3 = 1 - a_1 - a_2)$	0.32	0.37	0.49

a Gaussian onset with 600 fs full width at half-maximum, which represents the instrument response function.[11] Table 1 presents the results of the nonlinear least-squares fit.

The slow onset of photoconductivity in the epilayer sample ($\sim$3 ps) compared to that of the NPs results from carriers with about 1.6 eV of excess energy. The pump photons have 3.1 eV of energy, and the band gap is 1.35 eV, [18] but the vertical transition is not from the valence band maximum so the entire 1.75 eV excess energy is not available to the electrons. Nonetheless, the electrons are created high above the conduction band minimum, and they have sufficient energy to scatter into the lower mobility L and X valleys. The THz response, which is sensitive to carrier mobility, probes the population of carriers in the high mobility Γ valley. Detailed rate models incorporating relaxation of the carriers within the Γ valley, and scattering between the L, X and Γ valleys, have been successful in interpreting similar dynamics observed in GaAs.[10,23]

In contrast, the onset of the photoresponse of the NP arrays is much faster, limited by the instrument response time. Carriers excited in isolated NPs with excess energy quickly ($\sim$300 fs) relax to their lowest excited state,[24] and the arrays behave nearly identically to the isolated NPs. For the closely spaced NP arrays, the fastest time constant is 1.3 ps, which is longer than that for the arrays with 1.8 nm separation (0.4 ps), and it is 0.7 ps for the isolated NPs. Carrier trapping occurs predominately at the surface of the NPs, but the carriers scatter from the surface many times before trapping occurs.[12] The fact that the trapping time is lengthened for small interparticle separations indicates that the tunneling probability between NPs has increased, which is consistent with the enhanced THz absorption of the closely spaced arrays. The two longer time constants in the fit are also

greater for the closely spaced arrays. These time constants represent carrier trapping that occurs in NPs with a smaller number of surface defects. The fraction of e−h pairs that are rapidly trapped, given by the parameter a_1, is slightly decreased in the closely spaced arrays.

In conclusion, we observe a clear enhancement in the photoconductivity in arrays of 3.2 nm diameter InP NPs when their average separation is decreased from 1.8 to 0.9 nm. Understanding the onset of collective phenomena in such materials is essential. We have shown that TRTS is a new and powerful probe of the photoconductivity in these materials, and a more complete investigation of these observations is underway.

References

(1) Brus, L. E. *J. Chem. Phys.* **1984**, *80*, 4403−4409.
(2) Efros, A. L. *Sov. Phys. Semiconduct.* **1982**, *16*, 772−775.
(3) Alivisatos, A. P. *J. Phys. Chem.* **1996**, *100*, 13226−13239.
(4) Micic, O. I.; Ahrenkiel, S. P.; Nozik, A. J. *Appl. Phys. Lett.* **2001**, *78*, 4022−4024.
(5) Collier, C. P.; Saykally, R. J.; Shiang, J. J.; Henrichs, S. E.; Heath, J. R. *Science* **1997**, *277*, 1978−1981.
(6) Shiang, J. J.; Heath, J. R.; Collier, C. P.; Saykally, R. J. *J. Phys. Chem. B* **1998**, *102*, 3425−3430.
(7) Terrill, R. H.; Postlethwaite, T. A.; Chen, C. H.; Poon, C. D.; Terzis, A.; Chen, A. D.; Hutchison, J. E.; Clark, M. R.; Wignall, G.; Londono, J. D.; Superfine, R.; Falvo, M.; Johnson, C. S.; Samulski, E. T.; Murray, R. W. *J. Am. Chem. Soc.* **1995**, *117*, 12537−12548.
(8) Leatherdale, C. A.; Kagan, C. R.; Morgan, N. Y.; Empedocles, S. A.; Kastner, M. A.; Bawendi, M. G. *Phys. Rev. B* **2000**, *62*, 2669−2680.
(9) Smith, B. B.; Nozik, A. J. *Nano Lett.* **2001**, *1*, 36−41.
(10) Beard, M. C.; Turner, G. M.; Schmuttenmaer, C. A. *Phys. Rev. B* **2000**, *62*, 15764−15777.
(11) Beard, M. C.; Turner, G. M.; Schmuttenmaer, C. A. *J. Appl. Phys.* **2001**, *90*, 5915−5923.
(12) Beard, M. C.; Turner, G. M.; Schmuttenmaer, C. A. *Nano Lett.* **2002**, *2*, 983−987.
(13) Turner, G. M.; Beard, M. C.; Schmuttenmaer, C. A. *J. Phys. Chem. B* **2002**, *106*, 11716−11719.
(14) Leff, D. V.; Brandt, L.; Heath, J. R. *Langmuir* **1996**, *12*, 4723.
(15) Motte, L.; Pileni, M. P. *J. Phys. Chem. B* **1998**, 102, 4104.
(16) Kim, D. I.; Islam, M. A.; Avila, L.; Herman, I. P. *J. Phys. Chem. B* **2003**, 107, 6318.
(17) Nozik, A. J.; Micic, O. I. III−V Quantum Dots and Quantum Dot Arrays. In *Semiconductor Quantum Dots*; Klimov, V. I., Ed.; Marcel Dekker: New York, 2003.
(18) Yu, P. Y.; Cardona, M. *Fundamentals of Semiconductors*; Springer: New York, 2003.
(19) Ellingson, R. J.; Balckburn, J. L.; Yu, P.; Rumbles, G.; Micic, O. I; Nozik, A. J. *J. Phys. Chem.* 106, 7758, 2002.
(20) Smith, N. V. *Phys. Rev. B* **2001**, *64*, art. no.-155106.
(21) Mott, N. F. *Adv. Phys.* **1985**, *34*, 329−401.
(22) Lancefield, D. *Properties of Indium Phosphide*; INSPEC EMIS Datareviews Series No. 6; IEEE, 1991.
(23) Stanton, C. J.; Bailey, D. W. *Phys. Rev. B* **1992**, *45*, 8369−8377.
(24) Klimov, V. I.; McBranch, D. W. *Phys. Rev. Lett.* **1998**, *80*, 4028−4031.

NL0346777